ADDITIVE MANUFACTURING AND EXPERIMENTAL CHARACTERIZATION OF NICKEL-TITANIUM SHAPE-MEMORY ALLOY WICK STRUCTURES AND HEAT PIPES FOR SPACECRAFT THERMAL CONTROL

Tomé Seichi da Nóbrega Guenka, Reginald Hamilton, Christopher Greer, Sven Bilén, Na Liu, Bed Poudel, Alexander Rattner
The Pennsylvania State University, University Park, PA,16802

Ryan Overdorff
3D Systems Corporation, State College, PA, 16803

Bilal Bomani, William Sixel
NASA Glenn Research Center, Cleveland, OH, 44135

ABSTRACT

Shape memory alloys (SMA), such as those based on nickel-titanium (NiTi), are increasingly being applied as multifunctional spacecraft components. For thermal management applications, NiTi flow tubing hinges (Chong et al., 2018) and self-deploying loop heat pipes (Phillips & Ku, 2009) have been demonstrated. Emerging additive manufacturing (AM) processes are enabling more complex SMA devices than can be formed from conventional plain wire, tubing, and sheet stock materials. This paper presents our progress toward applying powder bed fusion AM to producing porous NiTi wicks and NiTi-H_2O heat pipes, which could be embedded in thermally deploying radiators for spacecraft thermal management. AM near-equiatomic NiTi (55.1 wt% Ni) porous wick specimens were produced with a range of deposition parameters. Transient acetone rate-of-rise experiments were performed to estimate wick permeability (K) and average pore radius (r_{pore}) values and identify parameter sets with high capillary performance. Surface treatments were evaluated to achieve hydrophilic wick structures. Evaluated treatments included chemical oxide growth with H_2O_2, oxide and sodium titanate growth with NaOH solution, and ultrasonic cleaning with specialty detergents that can remove hydrocarbon contaminants. The most durable hydrophilic surface conditions were obtained with the NaOH treatment. High performing wick deposition parameters were used to produce a full AM NiTi heat pipe, which was treated with NaOH solution to activate the wick. This heat pipe was operated on a test stand in the inverted configuration (upper evaporator and lower condenser), and demonstrated stable nearly isothermal operation for 150 hrs.

NOMENCLATURE, ACRONYMS, ABBREVIATIONS

A_c (m^2)	Cross-sectional area of the heat pipe
g (m s^{-2})	Earth's gravitational acceleration (9.81 m s^{-2})
h (m)	Water uptake height
h_{LV} (J kg^{-1})	Enthalpy of liquid-vapor phase change

K (m^2)	Permeability
P_{cap} (Pa)	Capillary pumping pressure $P_{cap} = 2\sigma \sin(\theta) / r_{pore}$
r_{pore} (m)	Pore radius

Greek Letters:

ϵ	Porosity
θ (degrees)	Contact angle
μ_L (kg m^{-1} s^{-1})	Liquid dynamic viscosity
ρ_L (kg m^{-3})	Liquid density
σ (kg s^{-2})	Fluid surface tension

1. INTRODUCTION

Shape memory alloys (SMA), such as those based on nickel-titanium (NiTi), are increasingly being applied in spacecraft as passive thermally driven actuators and superelastic flexure elements. In the thermal management context, NiTi flow tubing and heat pipes have been proposed as solutions for thermally conductive hinges. For example, coiled NiTi tubing has been demonstrated as a passively deploying condenser for loop heat pipe radiators (Phillips & Ku, 2009). Similarly, Chong *et al*. (2018) developed a variable conductance radiator concept that uses SMA tubes for fluid transport and as torque actuators. As NiTi alloys are challenging to machine, form, and join conventionally, such studies have focused on geometries that can be produced from plain wire, tubing, and sheets. Modern additive manufacturing (AM) processes are enabling production of geometrically complex functional SMA components (Elahinia et al., 2016; Wei et al., 2023) and porous structures (Lu et al., 2021). The focus of the present work is to apply these emerging capabilities to produce fully additively manufactured NiTi heat pipes with porous wicks. These could be embedded for mass efficient heat transfer in spacecraft systems, such as passive thermally-deploying heat rejection radiators.

Porous wick heat pipes are, conventionally, closed ended metal tubes with a thin internal layer of sintered powder wire or screens (the wick). In commissioning, such heat pipes are charged with working fluid that saturates the wick layer. During operation, heat input at one end (evaporator) causes liquid in the wick to evaporate and travel along the heat pipe. This flowing vapor stream condenses into the wick at the cooled end (condenser), and passively recirculates to the evaporator, driven by capillary action in the pore network of the wick. Because of the phase change and flow-based transport processes, heat pipes can achieve much greater equivalent axial thermal conductivity than solid metal sections, when operating under on-design conditions. Porous wick heat pipes can operate against accelerations and gravity (*i.e.*, wicking liquid upwards to an evaporator) and sustain relatively large evaporator heat fluxes compared with designs based on grooves or screen inserts. However, their overall heat transfer capacity and length can be limited by wick permeability (K, μm^2), capillary pressure ($P_{cap} = 2\sigma \cos\theta / r_{pore}$, Pa), or the combined wick performance metric K/r_{pore} (μm). For typical spacecraft equipment thermal management temperatures, water is considered a high-performance fluid because of its liquid-phase merit number for capillary heat transfer capacity (Merit number: $\rho_L \sigma_L h_{LV} / \mu_L$). However, water has poor wetting properties on the native surfaces of many candidate heat pipe materials (contact angle

$\theta \sim 70 - 90°$), such as titanium and NiTi. Surface treatments are generally needed to produce hydrophilic wicks with low contact angles.

The present study thus begins with a parametric study of laser powder bed fusion (LPBF) AM rastering parameters to produce NiTi (55.1 wt% Ni) wicks with high capillary performance (high K and K/r_{pore}). Transient liquid wicking "rate-of-rise" experiments are performed with acetone to indirectly measure the geometric K and r_{pore} values for these specimens. Treatments were then evaluated to improve hydrophilic properties of the wicks including ultrasonic cleaning in acetone and specialty detergent solutions, surface oxidation with hydrogen peroxide solution, and surface treatment in highly alkaline NaOH solution. A high-performance wick fabrication strategy and wettability treatment was then adopted to produce a full AM NiTi-H_2O heat pipe. The heat pipe was installed vertically in a test setup with a lower liquid-cooled heat sink (condenser) and an upper electrically heated collar (evaporator). Stable operation was observed over long duration testing (150 hrs), suggesting the feasibility of this AM NiTi heat pipe production approach for spacecraft thermal management.

2. ADDITIVE MANUFACTURING OF NITI POROUS WICK SPECIMENS

Porous rectangular coupons were additively manufactured through a LPBF process with a range of build parameters to identify high performance build strategies for NiTi wicks. These were fabricated using a 3D Systems DMP Flex 100 system equipped with a 100 W peak power laser. All coupons were produced using Fort Wayne Metals NiTi #5 powder. This material is reported to have 55.1 wt% Ni content and a median particle size of 45 μm.

The coupons had the following dimensions: 50 mm (z, vertical direction) × 10 mm × 4 mm (3 mm porous section, 1 mm solid backing). The porous sections were produced by laser scanning with relatively wide hatch spacings (275 and 400 μm vs. ~100 μm track width) and reduced laser power (56 – 93 W vs. 93 W solid-region baseline). Hatch scan directions were rotated 90° every 1, 3, or 6 layers to create inter-connected flow paths (Table 1). This strategy and parameter range for producing porous wicking structures was selected based on previous successful application to Inconel 718 and titanium wicking heat pipes (El Dannaoui et al., 2024; Noe et al., 2024).

Table 1: Printing parameters and raster patterns for rectangular wick coupons

Raster Line Spacing (μm)	Rastering Pattern	Laser Power (W, %)	Laser Scan Speed (mm s^{-1})	Layer Height (μm)
275 and 400	Rotating every 1, 3, or 6 layers between X and Y axes	56 (60%), 70 (75%), 84 (90%), 93 (100%)	950	30

Coupons are identified as Hxxx-Ly-Pzz, where xxx is the wick hatch spacing in microns, y is the number of build layers between each rotation of the rastering direction, and zz is the laser power percentage. Figure 1 shows the first batch of wick coupons. The wick sections of these samples were produced at 60% and 75% relative laser power levels. The 60% power level generally resulted in lack of fusion build failure, as documented in (Narasimharaju et al., 2022). Additionally, some of the wicks produced at 400 μm raster line spacing and 75% laser power had

visible defects. Specimen masses were used to estimate wick porosities, except for specimens with major defects.

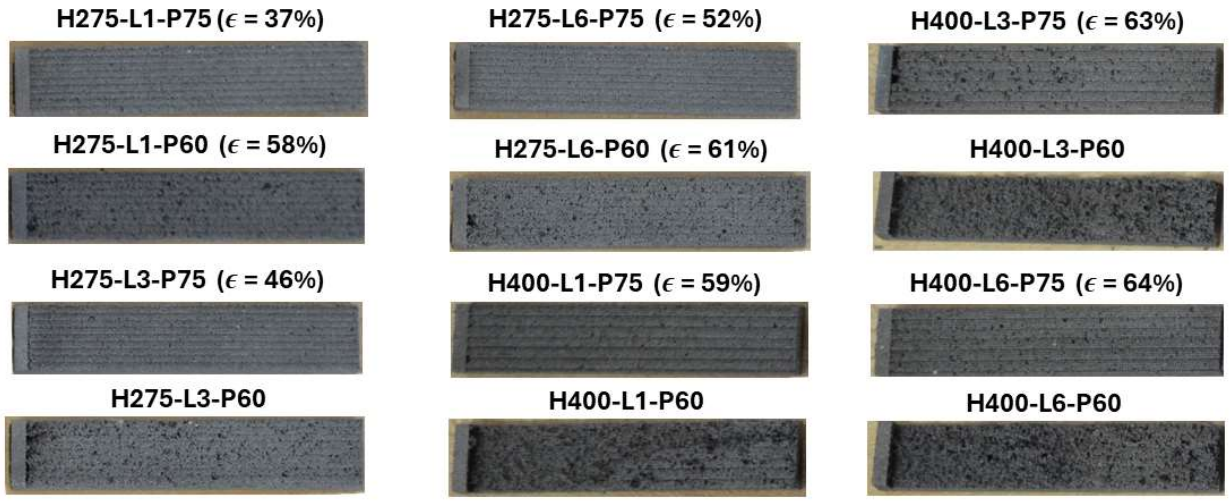

Figure 1: Photographs of wick coupons. Porosities (ϵ) based on dry coupon mass reported where feasible.

A second batch of coupons was produced with the same rastering parameters and increased laser power levels. The impacts of varying raster line spacing, layer alternation patterns, and laser power level can be assessed qualitatively in the side-by-side comparisons in Figure 2. Figure 2d

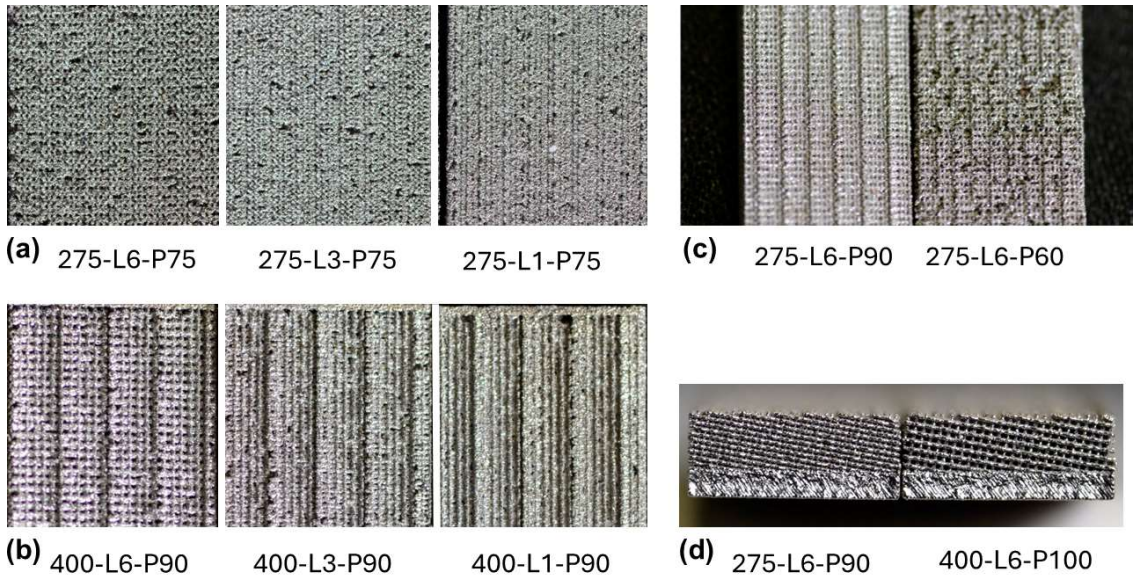

Figure 2: Wick coupouns produced with varying rastering parameters. (**a**) Comparison of 275 µm raster spacing coupons produced with different layer counts between rotations (**b**) Comparison of 400 µm raster spacing coupons produced with different layer counts between rotations. (**c**) Illustration of effect of varying laser power, with low power build (H275-60-6L) displaying many minor defects. (**d**) End-view illustrating range of pore sizes.

shows the visibly wider entrances to the wick channels of the 400 µm hatch spacing compared to the thinner channels in the 275 µm wick coupon. Two coupons printed with the same hatch spacing and alternation strategies but different laser power are shown in Figure 2c, where the wick manufactured at higher power has less defects in its structure than that manufactured at lower power. Thus, higher laser power (above 75 %) is necessary to achieve better wick integrity for the proposed material. After manufacturing, wick specimens were cleaned in an ultrasonic bath to remove un-sintered NiTi powder and other contaminants. The ultrasonic cleaning was performed in three stages with denatured alcohol, acetone, and deionized (DI) water, each for 5 minutes. After cleaning, all wick coupons were found to be slightly hydrophobic ($\theta > 90°$) with sessile water droplet tests.

3. RATE-OF-RISE EXPERIMENTS TO MEASURE WICK CAPILLARY PROPERTIES

A transient rate-of-rise (ROR) experimental approach was employed to evaluate the effective permeabilities (K) and average pore radius values (r_{pore}) of the manufactured wick coupons. It consists of a high-sensitivity cantilevered load cell rated for 100 g that suspends wick specimens above a working fluid container (acetone, Figure 3a). A wick specimen is initially slightly above the liquid free surface. Liquid is gradually added to the container until it meets the lower edge of the wick specimen. Transient weight data of the wick is logged as liquid climbs and saturated the wick. Permeability (K) and pore radius (r_{pore}) values are estimated from a non-linear fit of an analytic force balance model for capillary rise to transient experimental data (Eq. 1, Figure 3b).

$$\frac{\rho_L \epsilon}{2}\frac{d^2h(t)}{dt^2} = \frac{2\sigma\cos(\theta)\epsilon}{r_{pore}} - \frac{2\mu_L}{K}h(t)\frac{dh(t)}{dt} - (\rho_L g\epsilon)h(t) \quad (1)$$

Here σ is the liquid surface tension, θ is the working fluid contact angle with the studied surface, μ_L is the dynamic viscosity of the fluid, ϵ is the porosity of the wick (estimated from specimen dry mass), g is the acceleration of gravity, ρ_L is the fluid density, and $h(t)$ is the transient height of the liquid column rising into the wick. Here, porosity was measured based on the dry mass of wick coupons.

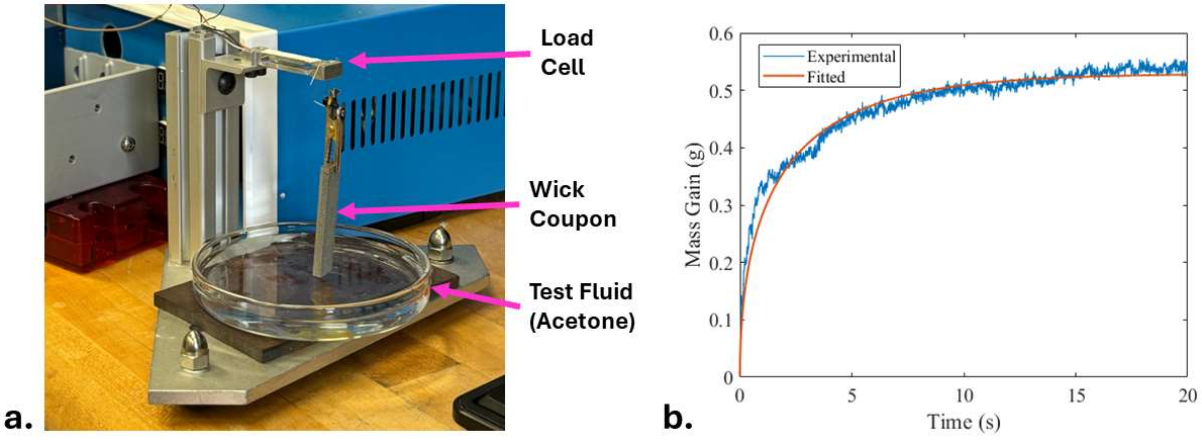

Figure 3: **a.** Transient rate of rise experimental set-up. **b**. Example of a best-fit capillary rise model to experimental measurements.

Results from the capillary rise experiments are summarized in Table 2. Here, values are averaged over three tests for each reported coupon except for H275-L1-60 (1 test) and H275-L6-P75 (2 tests). Because of the variable nature of the transient rate of rise experiments, K and r_{pore} values differed by up to ~60% for some specimens. Uncertainties are reported as 95% confidence intervals assuming normally distributed measurements. In general, K and K/r_{pore} values increased for more open wick structures with greater raster spacing and layer counts between raster direction rotations. On average, the H400-L1-P75 settings resulted in the greatest K/r_{pore} values. These were therefore adopted for the full heat pipe specimens described in Section 5.

Table 2: Rate of rise experiment results. Here, H is the raster line spacing, L is the number of layers between raster rotations, and P is the relative laser power (%). $\boldsymbol{K}$ and $\boldsymbol{r_{pore}}$ values are averaged over three tests except for H275-L1-60 (1 test) and H275-L6-P75 (2 tests).

Specimen	Porosity (ϵ, %)	Permeability (K, μm²)	Pore Radius (r_{pore}, μm)	K/r_{pore} (μm)
H275-L1-P75	37%	1170 ± 280	132 ± 25	8.8 ± 0.4
H275-L1-P60	58%	760	147	5.2
H275-L3-P75	46%	960 ± 120	148 ± 40	7.0 ± 2.3
H275-L6-P75	52%	1200 ± 190	133 ± 0	9.0 ± 1.4
H275-L6-P60	61%	1260 ± 240	153 ± 6	8.2 ± 1.3
H400-L1-P75	59%	2390 ± 150	170 ± 11	14.1 ± 0.4
H400-L3-P75	63%	2620 ± 780	187 ± 3	14.0 ± 3.9
H400-L6-P75	64%	2780 ± 360	204 ± 7	13.7 ± 2.1

4. SURFACE TREATMENTS AND CLEANING APPROACHES TO ACHIEVE HYDROPHILIC WICKS

For effective heat pipe operation with water, the AM NiTi wick surfaces must be modified from their non-wetting natural state to become hydrophilic. The selected treatment approaches must also be feasible to apply to the interior of a narrow heat pipe passage. This requirement precludes some common approaches for wettability enhancement, such as plasma treatment or laser etching (Jiang et al., 2022). Thermal treatments were excluded because the temperature ranges required for growing NiTi oxide layers could affect the SMA properties. Therefore, chemical treatments that modify surface chemistry (Samanta et al., 2021) and/or form hydrophilic nanostructures (Wemp & Carey, 2017) were sought.

The majority of published work on improving the hydrophilicity of NiTi substrates focuses on thermal treatments in air (Armitage et al., 2003; Michiardi et al., 2007) and chemical treatments (Chu et al., 2007; Martinez et al., 2023; Nazarov et al., 2021). These approaches can form oxide layers with greater thickness and different composition than the native titanium oxide layer that spontaneously forms on NiTi surfaces in air. Other studies have reported thermal and chemical treatments that produce complex hydrophilic nanostructures (Hang et al., 2019; Rao et al., 2012; Zhao et al., 2021). In all of these prior studies, NiTi samples were first polished (mechanically or chemically), which homogenizes surface topography and remove the native oxide layer (Chu et al., 2006; Chun et al., 2009), facilitating the target reactions. However, such pre-treatment may be

impractical to apply to porous wick structures or inside heat pipes. Instead of thermal treatment, Long *et al*. (2022) demonstrated that ultrasonic cleaning with suitable aqueous detergent solutions can remove hydrocarbon contaminants that rapidly passivate titanium surfaces. Such cleaning processes can offer temporary improvements in wettability in the ambient environment.

Based on these documented studies, four different treatments were evaluated to improve wettability of the AM NiTi wicks: (T1) solution treatment with hydrogen peroxide; (T2) solution treatment with concentrated NaOH solution; (T3) ultrasonic cleaning with a neutral pH aqueous detergent (Elma Lab Clean N10); and (T4) ultrasonic cleaning with a mildly alkaline aqueous detergent (Elma Tec Clean A4). The chemical solution treatments (T1: H_2O_2 and T2: NaOH) aimed to grow hydrophilic oxides, and were adapted from procedures by (Martinez et al., 2023; Rao et al., 2012; Zhao et al., 2021). In the H_2O_2 treatment, samples were submerged in a 33 wt% hydrogen peroxide solution bath at 60°C for 8 hours. In the NaOH treatment, specimens were submerged in a 15 M NaOH solution bath at room temperature (~21°C) for 24 hours. In the treatments T3 and T4, specimens were cleaned in ultrasonic baths at manufacturer-recommended detergent concentrations for 10 minutes at ~45°C. Specimens were then thoroughly rinsed with deionized (DI) water. In the work of Long *et al*. (2022), cleaning with similar specialty detergents was found to remove hydrocarbon contaminants that could not be removed with organic solvents.

Sessile droplet tests were performed for treated specimens to assess wettability changes. None of the samples treated with H_2O_2 (T1) visibly wicked water ($\theta > 90°$). The NaOH solution (T2) and both detergents (T3 and T4) clearly improved wettability, with deposited water droplets rapidly soaking into wick structures immediately after treatment. Wettability improvements with the NaOH treatment were found to persist for over a week for specimens stored in the laboratory environment, suggesting relatively durable hydrophilic properties. A risk with this approach is that NaOH deposits could be challenging to clean from the interior of long heat pipes and could partially block wick pores or cause long-term corrosion. The detergent cleaned specimens were found to revert to non-wetting after ~48 hrs of storage in the laboratory environment. However, such cleaning treatments might produce persistent wetting properties inside sealed heat pipes. These findings are summarized qualitatively in Table 3.

Table 3: Summary of surface treatment methods and wettability results from sessile droplet tests.

Treatment	Results
T1: H_2O_2 chemical treatment	Did not significantly improve wettability. Surface color change was noticed
T2: NaOH chemical treatment	Improved wettability, with hydrophilicity lasting for over a week
T3. Neutral detergent cleaning	Improved wettability with hydrophilicity lasting around 48 hours when stored properly
T4. Alkaline detergent cleaning	

5. HEAT PIPE PRODUCTION AND TESTING

A cylindrical heat pipe was additively manufactured in NiTi with 6 mm outer diameter and overall length of 60 mm. The outer shell of the heat pipe was 300 µm thick and closed at one end. The inside of the heat pipe was lined with a 900 µm thick wick layer produced with the H400-L1-P75 parameters. These rastering parameters were selected because they yielded the consistently highest permeability (K = 2200 – 2400 µm^2) and permeability-to-pore radius ratio (K/r_{pore} = 14 µm) values of tested wicks. The open end of the heat pipe specimen was machined to install a valve for liquid water charging and vacuum degassing.

An experimental setup was prepared to test the heat pipe operation (Figure 4). The heat pipe and charging valve were mounted vertically. A copper collar with an electrical cartridge heater was clamped at the top of the heat pipe (evaporator). A liquid-cooled copper heat sink was clamped to the bottom end of the heat pipe (condenser). The copper evaporator and condenser blocks had embedded thermocouples to measure temperature. The adiabatic section of the heat

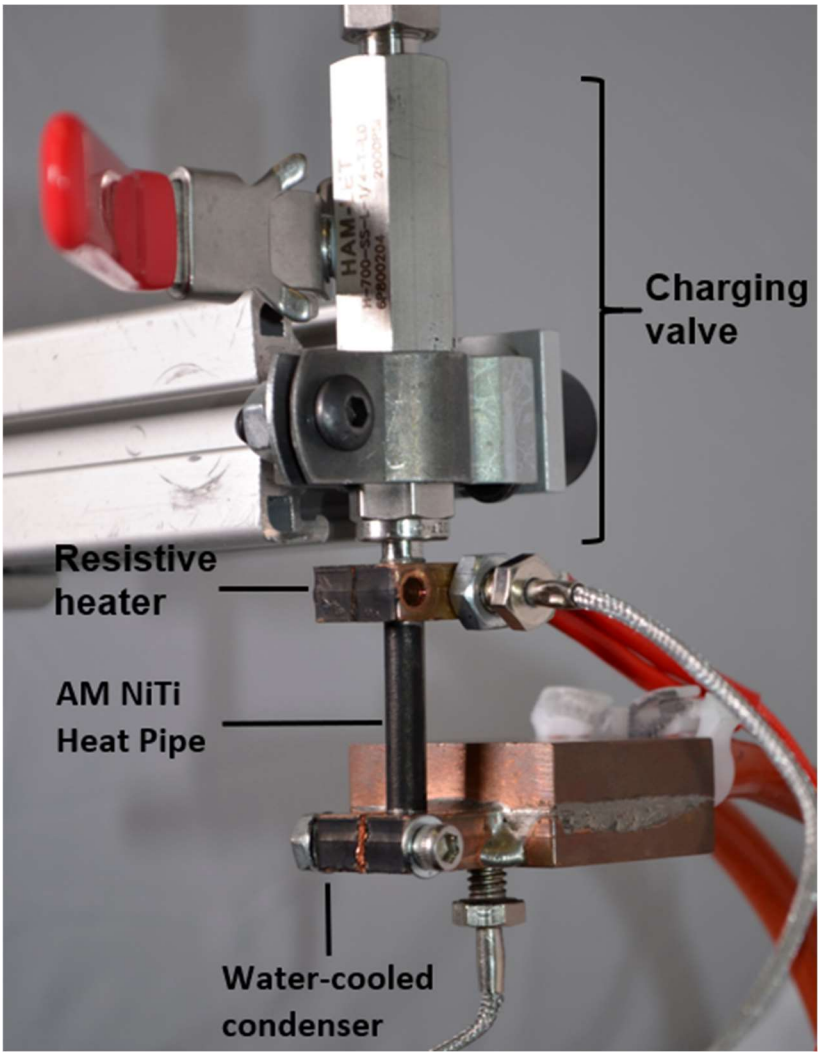

Figure 4: Photograph of heat pipe test setup.

pipe between the copper heat transfer components was 26 mm long. The surface of the heat pipe was painted flat black for thermal imaging (IR) measurement of the surface temperature profile.

Initially, the heat pipe was ultrasonically cleaned with the alkaline detergent (Elma Tec Clean A4) and charged with 1-2 ml of water. The heater power was set to 3.6 W (~90°C block temperature), and the condenser was cooled with 15°C water flow. Vacuum was cyclically applied through the valve until the IR temperature profile appeared uniform along the adiabatic section. After about an hour of operation at this condition, the axial temperature profile gradually transitioned to linear between the evaporator and condenser temperatures. It was suspected that the wick surface could have become contaminated and non-wetting, even in the relatively sealed assembly. However, minor leaks on the valve and fitting could have also contributed to the degradation.

The heat pipe was then treated with concentrated NaOH solution and then flushed with DI water to produce a more durable hydrophilic surface state. The specimen was re-installed in the test stand and charged and operated as before. After reassembling the experimental setup with the treated heat pipe, the same conditions were set as in the prior testing. In this second cycle, the heat pipe maintained stable, nearly isothermal operation between the condenser and evaporator temperatures for a continuous run of 150 hrs (Figure 5).

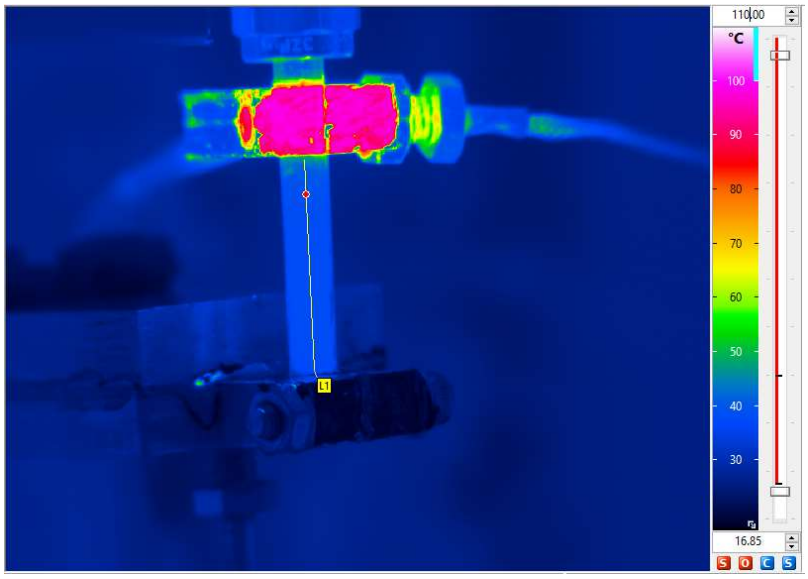

Figure 5: Thermal image of heat pipe operating between lower liquid cooled condenser at 15°C and upper electrically heated evaporator. Sustained nearly isothermal operation was observed for a continuous 150 hr test.

6. CONCLUSIONS

In this study, a parametric study of rastering parameters was conducted to produce NiTi porous wick structures through powder bed fusion additive manufacturing. Transient liquid rate of rise experiments with acetone were conducted to estimate properties of the wicks (K and r_{pore}), and

identify parameter sets with high capillary performance. Chemical (H_2O_2 and NaOH) solution treatments and ultrasonic cleaning with specialty detergents were evaluated to improve hydrophilic properties of the wicks. It was found that the selected detergents improved wetting temporarily, and the NaOH treatment resulted in durable hydrophilic surface conditions that persisted for over a week in the laboratory environment.

A full NiTi heat pipe was additively manufactured with an internal porous wick employing high performing parameters identified in the rate-of-rise testing. The heat pipe was mounted in a thermal test stand with an upper electrically heated evaporator and lower liquid cooled condenser. With the NaOH wettability treatment, this specimen maintained nearly isothermal profile for a 150 hour continuous test.

In planned work, an integrated AM NiTi heat pipe assembly will be prepared with additional instrumentation and insulation to more precisely measure thermal performance. Mechanically compliant NiTi heat pipe geometries will also be explored for applications such as heat rejection radiator panels that can passively deploy via the shape-memory effect.

ACKNOWLEDGEMENTS

The authors wish to acknowledge generous support from the U.S. National Aeronautics and Space Agency Space Technology Mission Directorate through the Small Spacecraft Technology (SST) program (Grant 80NSSC23M0234).

REFERENCES

Armitage, D. A., Parker, T. L., & Grant, D. M. (2003). Biocompatibility and hemocompatibility of surface-modified NiTi alloys. *Journal of Biomedical Materials Research - Part A*, *66*(1), 129–137. https://doi.org/10.1002/jbm.a.10549

Chong, J. B., Walgren, P. P., & Hartl, D. J. (2018). *Demonstration of a shape memory alloy torque tube-based morphing radiator*. 90. https://doi.org/10.1117/12.2300818

Chu, C. L., Chung, C. Y., & Chu, P. K. (2006). Surface oxidation of NiTi shape memory alloy in a boiling aqueous solution containing hydrogen peroxide. *Materials Science and Engineering: A*, *417*(1–2), 104–109. https://doi.org/10.1016/j.msea.2005.11.010

Chu, C. L., Hu, T., Wu, S. L., Dong, Y. S., Yin, L. H., Pu, Y. P., Lin, P. H., Chung, C. Y., Yeung, K. W. K., & Chu, P. K. (2007). Surface structure and properties of biomedical NiTi shape memory alloy after Fenton's oxidation. *Acta Biomaterialia*, *3*(5), 795–806. https://doi.org/10.1016/j.actbio.2007.03.002

Chun, Y., Levi, D. S., Mohanchandra, K. P., & Carman, G. P. (2009). Superhydrophilic surface treatment for thin film NiTi vascular applications. *Materials Science and Engineering C*, *29*(8), 2436–2441. https://doi.org/10.1016/j.msec.2009.07.004

El Dannaoui, T., Noe, C., Bhate, D., Greer, C., Bilén, S., Ramos Alvarado, B., Sixel, W., & Rattner, A. (2024). *Production and characterization of additively manufactured radiator panels with integral branching heat pipes for high-temperature heat rejection*. Thermal & Fluids Analysis Workshop, Cleveland, Ohio.

Elahinia, M., Shayesteh Moghaddam, N., Taheri Andani, M., Amerinatanzi, A., Bimber, B. A., & Hamilton, R. F. (2016). Fabrication of NiTi through additive manufacturing: A review. *Progress in Materials Science*, *83*, 630–663. https://doi.org/10.1016/j.pmatsci.2016.08.001

Hang, R., Liu, S., Liu, Y., Zhao, Y., Bai, L., Jin, M., Zhang, X., Huang, X., Yao, X., & Tang, B. (2019). Preparation, characterization, corrosion behavior and cytocompatibility of NiTiO 3 nanosheets hydrothermally synthesized on biomedical NiTi alloy. *Materials Science and Engineering C*, *97*, 715–722. https://doi.org/10.1016/j.msec.2018.12.124

Jiang, G., Tian, Z., Luo, X., Chen, C., Hu, X., Wang, L., Peng, R., Zhang, H., & Zhong, M. (2022). Ultrathin aluminum wick with dual-scale microgrooves for enhanced capillary performance. *International Journal of Heat and Mass Transfer*, *190*. https://doi.org/10.1016/j.ijheatmasstransfer.2022.122762

Long, J., Li, Y., Ouyang, Z., Xi, M., Wu, J., Lin, J., & Xie, X. (2022). A universal approach to recover the original superhydrophilicity of micro/nano-textured metal or metal oxide surfaces. *Journal of Colloid and Interface Science*, *628*, 534–544. https://doi.org/10.1016/j.jcis.2022.08.039

Lu, H. Z., Ma, H. W., Luo, X., Wang, Y., Wang, J., Lupoi, R., Yin, S., & Yang, C. (2021). Microstructure, shape memory properties, and in vitro biocompatibility of porous NiTi scaffolds fabricated via selective laser melting. *Journal of Materials Research and Technology*, *15*, 6797–6812. https://doi.org/10.1016/j.jmrt.2021.11.112

Martinez, A. L., Saugo, M., Flamini, D. O., & Saidman, S. B. (2023). Enhancing the corrosion behavior of Ti–6Al–4V and Nitinol alloys by simple chemical oxidation in H2O2. *Materials Chemistry and Physics*, *295*. https://doi.org/10.1016/j.matchemphys.2022.127069

Michiardi, A., Aparicio, C., Ratner, B. D., Planell, J. A., & Gil, J. (2007). The influence of surface energy on competitive protein adsorption on oxidized NiTi surfaces. *Biomaterials*, *28*(4), 586–594. https://doi.org/10.1016/j.biomaterials.2006.09.040

Narasimharaju, S. R., Zeng, W., See, T. L., Zhu, Z., Scott, P., Jiang, X., & Lou, S. (2022). A comprehensive review on laser powder bed fusion of steels: Processing, microstructure, defects and control methods, mechanical properties, current challenges and future trends. *Journal of Manufacturing Processes*, *75*, 375–414. https://doi.org/10.1016/j.jmapro.2021.12.033

Nazarov, D., Rudakova, A., Borisov, E., & Popovich, A. (2021). Surface modification of additively manufactured nitinol by wet chemical etching. *Materials*, *14*(24). https://doi.org/10.3390/ma14247683

Noe, C., Morankar, S., Rattner, A. S., Potts, A., Goode, Z., Dannaoui, T. E., Sherbondy, J. R., Chawla, N., Sixel, W., Bilén, S., Lynch, S., Westover, C., & Bhate, D. (2024). *Structured, Sintered, and Rastered Strategies for Fluid Wicking in Additively Manufactured Heat Pipes*.

Phillips, A. L., & Ku, J. (2009). *Self Deploying Nitinol LHP Radiator for Small Spacecraft*. 23rd Annual AIAA/USU Conference on Small Satellite.

Rao, X., Chu, C. L., Chung, C. Y., & Chu, P. K. (2012). Hydrothermal growth mechanism of controllable hydrophilic titanate nanostructures on medical niti shape memory alloy. *Journal of Materials Engineering and Performance*, *21*(12), 2600–2606. https://doi.org/10.1007/s11665-012-0267-3

Samanta, A., Huang, W., Parveg, A. S. M. S., Kotak, P., Auyeung, R. C. Y., Charipar, N. A., Shaw, S. K., Ratner, A., Lamuta, C., & Ding, H. (2021). Enabling Superhydrophobicity-Guided Superwicking in Metal Alloys via a Nanosecond Laser-Based Surface Treatment Method. *ACS Applied Materials and Interfaces*, *13*(34), 41209–41219. https://doi.org/10.1021/acsami.1c09144

Wei, S., Zhang, J., Zhang, L., Zhang, Y., Song, B., Wang, X., Fan, J., Liu, Q., & Shi, Y. (2023). Laser powder bed fusion additive manufacturing of NiTi shape memory alloys: A review. *International Journal of Extreme Manufacturing*, *5*(3). https://doi.org/10.1088/2631-7990/acc7d9

Wemp, C. K., & Carey, V. P. (2017). Water Wicking and Droplet Spreading on Randomly Structured Thin Nanoporous Layers. *Langmuir*, *33*(50), 14513–14525. https://doi.org/10.1021/acs.langmuir.7b03687

Zhao, Y., Bai, L., Sun, Y., Yao, X., Huang, X., Hang, R., & Huang, D. (2021). Low-temperature alkali corrosion induced growth of nanosheet layers on NiTi alloy and their corrosion behavior and biological responses. *Corrosion Science*, *190*. https://doi.org/10.1016/j.corsci.2021.109654